

Measurements of neutron-deuteron elastic and charge exchange scattering

X. H. Chen, C. Dupont, P. Leleux, P. Lipnik, P. Macq, and A. Ninane
Institut de Physique, Université Catholique de Louvain, B-1348 Louvain-la-Neuve, Belgium
 (Received 15 July 1985)

The neutron-deuteron elastic scattering cross section was measured at 90° and 166° center of mass, at 31, 61, and 76 MeV. The charge exchange reaction ${}^2\text{H}(n,p)\text{nn}$ was measured at 7° laboratory for the same energies; the ratio of the latter to the neutron-proton elastic scattering was inferred.

Contrary to the proton-deuteron (p-d) reaction which was widely studied, there exists only scarce data for the neutron-deuteron (n-d) reaction; in particular, there is a large gap between 46 and 130 MeV with no published data.¹ In parallel to a recent measurement² of the neutron-proton (n-p) elastic scattering at backward center-of-mass (c.m.) angles and at 90° c.m., cross sections were also measured for the n-d elastic ${}^2\text{H}(n,d)\text{n}$ and charge exchange ${}^2\text{H}(n,p)\text{nn}$ scattering at three energies: 31.3, 60.9, and 76.2 MeV, at deuteron and proton laboratory angles of 7° and 45°.

The experimental setup was already described.² In brief, a neutron beam is produced at 0° by the Li(p,n) reaction induced by a 5-μA proton beam from the Louvain isochronous cyclotron. Behind the target, protons are bent downwards and collected in a carbon Faraday cup. An iron collimator defines a 2-cm-diameter field at 6.7 m from the target. At that place, neutrons interact with a 5-mm-thick liquid deuterium target limited by 6-μm-thick aluminized Mylar windows. Charged particles contaminating the neutron beam are vetoed by a 0.1-mm-thick plastic scintillator (VETO) in front of the deuterium target. Immediately behind the target, recoil charged particles fire a 0.1-mm plastic scintillator (START) which has two purposes: (i) to measure the incident neutron energy by time of flight (TOF) with respect to a capacitive beam pickoff (BPO) located upstream of the Li target, and (ii) to generate the energy spectrum of the recoil charged particles by TOF with two 3-cm-diameter, 1-mm-thick plastic scintillators (STOP) set at 7° and 45° at 1 m from the deuterium target. Behind

each STOP detector, a copper absorber eliminates low-energy protons from deuteron breakup, while elastic deuterons are transmitted. Each absorber is followed by a 4-cm-diameter and 1-mm-thick plastic scintillator (D) in coincidence with the corresponding STOP detector. Apart from the three TOF, the amplitude spectrum of each scintillator is also recorded. All the data are CAMAC coded and stored on magnetic tape. A CAMAC gate is defined as $\text{START} \times \text{BPO} \times [(\text{STOP} \times D)_{7^\circ} \text{ or } (\text{STOP} \times D)_{45^\circ}]$. Runs are alternated for a deuterium and an empty target, and normalized to the Faraday cup integrated current. The target is filled with liquid hydrogen for the normalization runs to the n-p elastic scattering; the pressure over the liquid is kept the same for both isotopes. The quantity of gas injected into the target is monitored by a calibrated flowmeter. The setup is drawn in Fig. 1.

The data analysis proceeds as follows: the START-BPO spectrum is used to select the high-energy neutron peak. A low-energy cut is then applied on the STOP amplitude spectra and the START-STOP TOF spectra at 7° and 45° are reconstructed. In each one (Fig. 2), for the case of a deuterium target, two peaks are integrated, namely, the elastic deuteron peak and the quasielastic proton peak. The signal-to-noise ratio is larger than six. The solid angle of the STOP detectors was measured with an α source of known activity. The proton and deuteron loss due to reac-

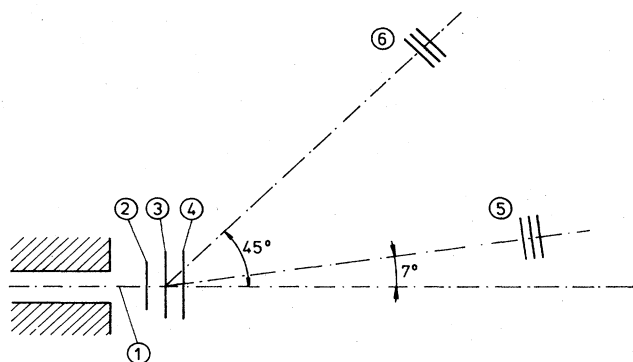


FIG. 1. Experimental setup. 1 is the collimated neutron beam; 2 is the veto detector; 3 is the liquid deuterium target; 4 is the start detector; 5 or 6 is the stop detector + copper absorber + D detector. The distance from 3 to 5 or 6 is 1 m.

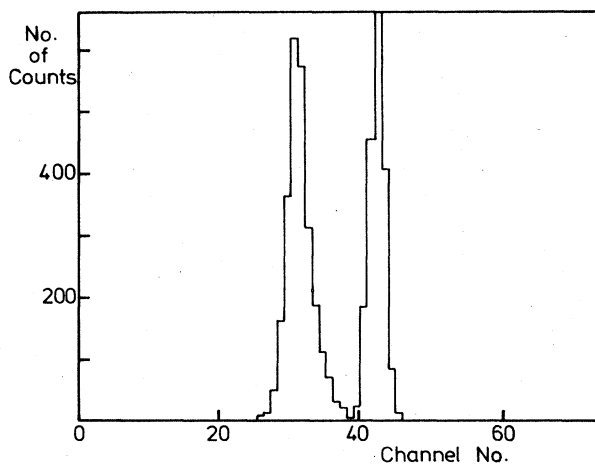


FIG. 2. Start-stop TOF spectrum at 7° laboratory at $E_n = 61$ MeV, showing the charge exchange proton peak and the elastic deuteron peak. The horizontal scale is 0.4 ns/channel.

TABLE I. Measured n-d elastic cross section in the c.m. system.

E_n (MeV)	Cross section (mb/sr)	
	90°	166°
31.3 ± 2.1	...	22.90 ± 1.50
60.9 ± 2.5	1.14 ± 0.16	6.18 ± 0.24
76.2 ± 2.2	0.93 ± 0.05	4.02 ± 0.19

tions in the STOP scintillator and in the copper absorber are taken into account. The deuteron data are normalized to the n-p elastic scattering at 90°, taken from a recent global (0–1 GeV) phase shift analysis.³ Table I quotes the measured n-d elastic cross sections at 166° and 90° c.m. The quoted error is statistical only. Nonstatistical errors arise from the solid angle determination (1.1%) and from the normalization to the n-p cross section ($\leq 3\%$).⁴

The 166° n-d elastic cross section data from this work are plotted in Fig. 3, together with results from Karlsruhe, Davis, Harwell, and Harvard,⁵ in a log-log diagram. The angular distributions of Ref. 5 were first separately fitted with a Legendre polynomial series to obtain cross sections at

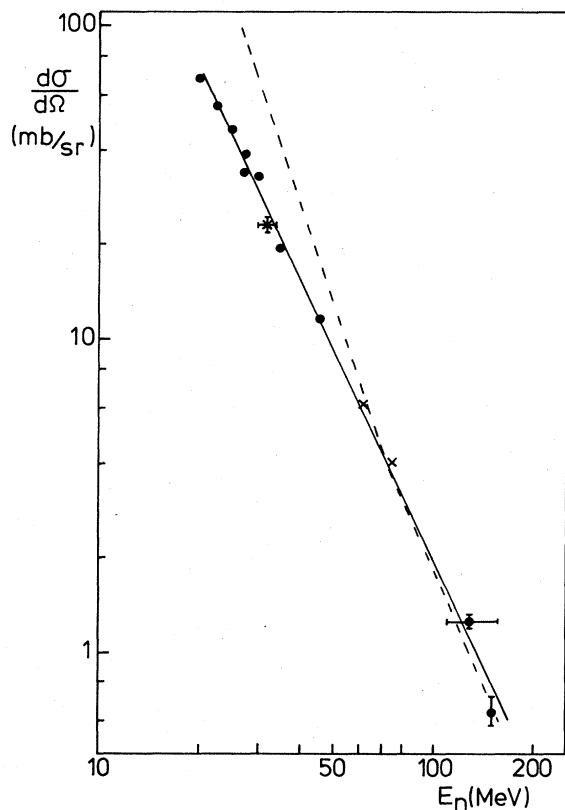


FIG. 3. The n-d elastic cross section at 166° c.m. vs the laboratory neutron energy (crosses are our data; dots are data from Ref. 5). The solid line is a linear fit to the data. The dotted line shows the trend of the p-d data at the same angle (Ref. 6).

TABLE II. Ratio R of the ${}^2\text{H}(n,p)nn$ to the ${}^1\text{H}(n,p)n$ reaction at 7° laboratory angle.

E_n (MeV)	R
31.3 ± 2.1	0.42 ± 0.05
60.9 ± 2.5	0.56 ± 0.03
76.2 ± 2.2	0.65 ± 0.04

166° precisely. In Fig. 3 the c.m. elastic cross section is plotted versus the laboratory energy in a log-log diagram. A linear fit with a slope of -2.2 reproduces satisfactorily the n-d data. The trend of the p-d elastic cross section data at the same angle⁶ is also drawn; both curves meet only above 80 MeV, which emphasizes the importance of Coulomb effects at backward angles in the three-body problem.

The n-d charge exchange ${}^2\text{H}(n,p)nn$ reaction at forward proton laboratory angle is usually compared with the n-p elastic scattering at backward c.m. angle (which is equivalent to a scattered proton at forward laboratory angle). Because of the Pauli principle, which forbids some di-neutron final states in the n-d charge exchange reaction, it is expected⁷ that the ratio R of the latter cross section to the n-p elastic cross section will be smaller than one. Even if the deuteron binding energy is neglected, a meaningful comparison of both processes should be done only at 0° laboratory, i.e., at the angle where the energy of the struck proton is the same in both cases. Measurements at 0° are scarce (the most recent and precise data point is $R = 0.56 \pm 0.04$ at 794 MeV).⁸ At larger proton laboratory angles, the two outgoing neutrons carrying a nonzero relative energy are no more restricted to be in a 1S_0 state, and R should be larger. Table II quotes the measured R in this work at 7° laboratory angle. Figure 4 shows R versus the neutron energy for proton laboratory angles close to 7° (in fact, from 4° to 10°). Our data fill a gap in an energy region of strong variation of R . Other data are from Refs. 8 and 9. The ratio seems to saturate around 100 MeV, indicating that above this energy, the neutron sees the deuteron as a target of free neutron and proton. However, the R data above 700 MeV are slightly larger and the trend of R from 400 to 700 MeV is unknown.

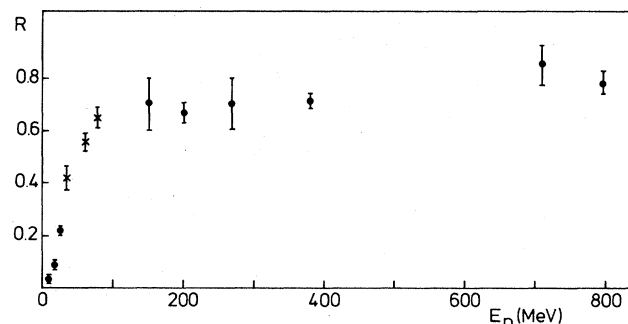


FIG. 4. Ratio (R) of the charge exchange ${}^2\text{H}(n,p)nn$ to the elastic ${}^1\text{H}(n,p)n$ scattering at about 7° laboratory proton angle. The crosses are our data, the dots are from Refs. 8 and 9.

This work was supported in part by the Institut Interuniversitaire des Sciences Nucléaires, Belgium. We wish to thank the cyclotron staff for efficiently running the machine. Two of us (P.Le. and A.N.) thank the National Fund for Scientific Research, Belgium, for financial support.

¹The Davis group has done measurements of the n-d elastic scattering at 54, 59.6, and 63 MeV, which were mentioned in progress reports but were not published.

²A. Bol *et al.*, Phys. Rev. C **32**, 308 (1985).

³R. A. Arndt and L. D. Roper, N-N interactive program (private communication).

⁴C. Dupont *et al.*, Nucl. Phys. (to be published).

⁵P. Schwarz *et al.*, Nucl. Phys. **A398**, 1 (1983); F. P. Brady *et al.*, Phys. Rev. C **9**, 1784 (1974); V. J. Howard *et al.*, Nucl. Phys. **A218**, 140 (1974); J. N. Palmieri, *ibid.* **A188**, 72 (1972).

⁶S. N. Bunker *et al.*, Nucl. Phys. **A113**, 461 (1968); C. C. Kim *et al.*, *ibid.* **58**, 32 (1964); M. Davison *et al.*, *ibid.* **45**, 423 (1963);

O. Chamberlain and M. O. Stern, Phys. Rev. **94**, 666 (1954); H. Postma and R. Wilson, *ibid.* **121**, 1229 (1961); K. Kuroda *et al.*, Nucl. Phys. **88**, 33 (1966); G. Igo *et al.*, *ibid.* **A195**, 33 (1972).

⁷G. Chew, Phys. Rev. **84**, 710 (1951).

⁸B. E. Bonner *et al.*, Phys. Rev. C **17**, 664 (1978).

⁹K. Debertin *et al.*, Nucl. Phys. **81**, 220 (1966); M. Cerineo *et al.*, Phys. Rev. B **133**, 948 (1964); D. F. Measday, Phys. Lett. **21**, 66 (1966); A. R. Thomas *et al.*, Phys. Rev. **167**, 1240 (1968); J. B. Cladis *et al.*, *ibid.* **86**, 110 (1952); V. P. Dzelopov and S. A. Sestopalova, Nuovo Cimento **1**, 61 (1956); R. R. Larsen, *ibid.* **18**, 1039 (1960).